nature geoscience

LETTERS

PUBLISHED ONLINE: 8 MAY 2011 | DOI: 10.1038/NGEO1148

Hydrothermal vents as a kinetically stable source of iron-sulphide-bearing nanoparticles to the ocean

Mustafa Yücel[1,3]*, Amy Gartman[1], Clara S. Chan[2] and George W. Luther III[1]*

Hydrothermal vents emit sulphur and metals to the ocean[1]. Particular attention has been paid to hydrothermal fluxes of iron[2–4], a limiting micronutrient of marine primary production[5]. Vent-derived iron was previously thought to rapidly oxidize and precipitate around vents[6]. However, organic matter can bind to and stabilize dissolved and particulate iron in hydrothermal plumes[7–9], facilitating its dispersion into the open ocean[10]. Here, we report measurements of the chemical speciation of sulphide and iron in high-temperature fluids emanating from vents in the East Pacific Rise and the Eastern Lau Spreading Center. We show that pyrite nanoparticles—composed of iron and sulphur—account for up to 10% of the filterable iron (less than 200 nm in size) in these fluids. We suggest that these particles form before the discharge of the vent fluid. We estimate that pyrite nanoparticles sink more slowly than larger plume particles, and are more resistant to oxidation than dissolved Fe(II) and FeS. We suggest that the discharge of iron in the form of pyrite nanoparticles increases the probability that vent-derived iron will be transported over long distances in the deep ocean.

Increasing efforts have been invested recently to provide improved estimates of dissolved iron fluxes from deep-sea hydrothermal vents into the ocean[3]. Moreover, the importance of vent-derived iron for global ocean biogeochemistry has been debated, as iron is a vital micronutrient for plankton and bacteria in remote parts of the ocean[5]. Researchers have suggested that hydrothermal vents could be responsible for a dissolved Fe flux approximately equal to the flux from rivers[11]. However, analogous to the processes that trap riverine iron in estuaries and continental shelves, mixing of hot vent fluid with cold, oxic seawater causes particulate iron formation and subsequent storage of iron around vent fields[12]. Still, an unknown fraction of this flux escapes from precipitation, as enrichment of dissolved iron was reported to be as much as several hundred nanomolar in hydrothermal plumes[7,13]. This enrichment was recently attributed to the presence of organic ligands, as plumes entrain the organic matter that is present at high concentrations around hydrothermal vent ecosystems[9]. Recent modelling work also concluded that the inclusion of hydrothermal iron flux is necessary to explain recently observed dissolved iron distributions in the Southern Ocean[4]. In the South Pacific, a hydrothermal source was attributed to the 50% increase in Fe over background, the Fe anomaly, and the δ^3He increase at depths from 1 to 5 km (ref. 10).

Sulphide and metal speciation in the source high-temperature fluids has attracted little attention in previous work but can have a major influence on the fate of vent-derived metals in the deep ocean and their availability to organisms, similar to recent reports for diffuse flow vent fluids[14,15]. Dissolved sulphide was generally thought to exist merely as H_2S in high temperature vent fluids, with FeS and FeS_2 precipitating only after the vent fluid mixes with ambient seawater[16]. Here we report sulphide and iron speciation in unfiltered and filtered (200 nm) source high-temperature vent fluids collected with titanium samplers[17] from two different vent fields, East Pacific Rise (EPR), 9° 50′ N, and Eastern Lau Spreading Center in the Lau Basin (Southwest Pacific Ocean). We show that FeS_2 nanoparticles (<200 nm) have already formed in the high temperature–pressure conditions in the upflow zone before the discharge of the vent fluid. Thus, a substantial fraction of the iron entering the ocean from vents is already in a stable form as nanoparticulate FeS_2, where Fe^{2+} is in the low spin d^6 state and thus stable to dissociation.

In our sulphide speciation scheme, free H_2S and FeS in the vent fluids can be quantitatively fixed as ZnS and later recovered by acidification (3 M HCl) to give acid-volatile sulphides (AVS). After this leach, the remaining sulphide in the sample can be measured after a short (1 h) cold chromium(II) reduction analogous to sediment leaches[18]. Chromium(II) attacks disulphide bonds and, given the abundance of dissolved iron and sulphide in vent fluids, FeS_2 crystals/nanoparticles are the most likely chemical species that make up chromium-reducible sulphides (CRS) in our samples. AVS concentrations (Fig. 1a,c) did not vary much between the filtered and unfiltered fractions, confirming that 'free' H_2S and FeS clusters/nanoparticles make up this fraction. CRS was detected in all samples analysed, always being much higher in unfiltered samples (Fig. 1b,d). Significant CRS concentrations were measured after filtering the sample through 200 nm filters, indicating the presence of <200 nm sulphide nanoparticles. For filtered samples, the <200 nm CRS nanoparticles can make up a significant fraction (up to 11%) of total dissolved sulphide in both EPR and Lau samples.

In our May/June 2009 expedition to Lau Basin, Fe measurements were made to test that CRS consists of pyrite (nano)particles. In addition to the detection of dissolved Fe by the ferrozine method[19] in samples acidified with HCl, unfiltered and filtered samples were treated with an aliquot of concentrated nitric acid, which is

[1]University of Delaware, School of Marine Science and Policy, College of Earth, Ocean and Environment, Lewes, Delaware 19958, USA, [2]Department of Geological Sciences, Newark, Delaware 19711, USA, [3]Present address: Université Pierre et Marie Curie—Paris 6, Benthic Ecogeochemistry Laboratory (CNRS UPMC FRE3350), Observatoire Océanologique de Banyuls, 66651 Banyuls-sur-mer, France. *e-mail: yucel@obs-banyuls.fr; luther@udel.edu.

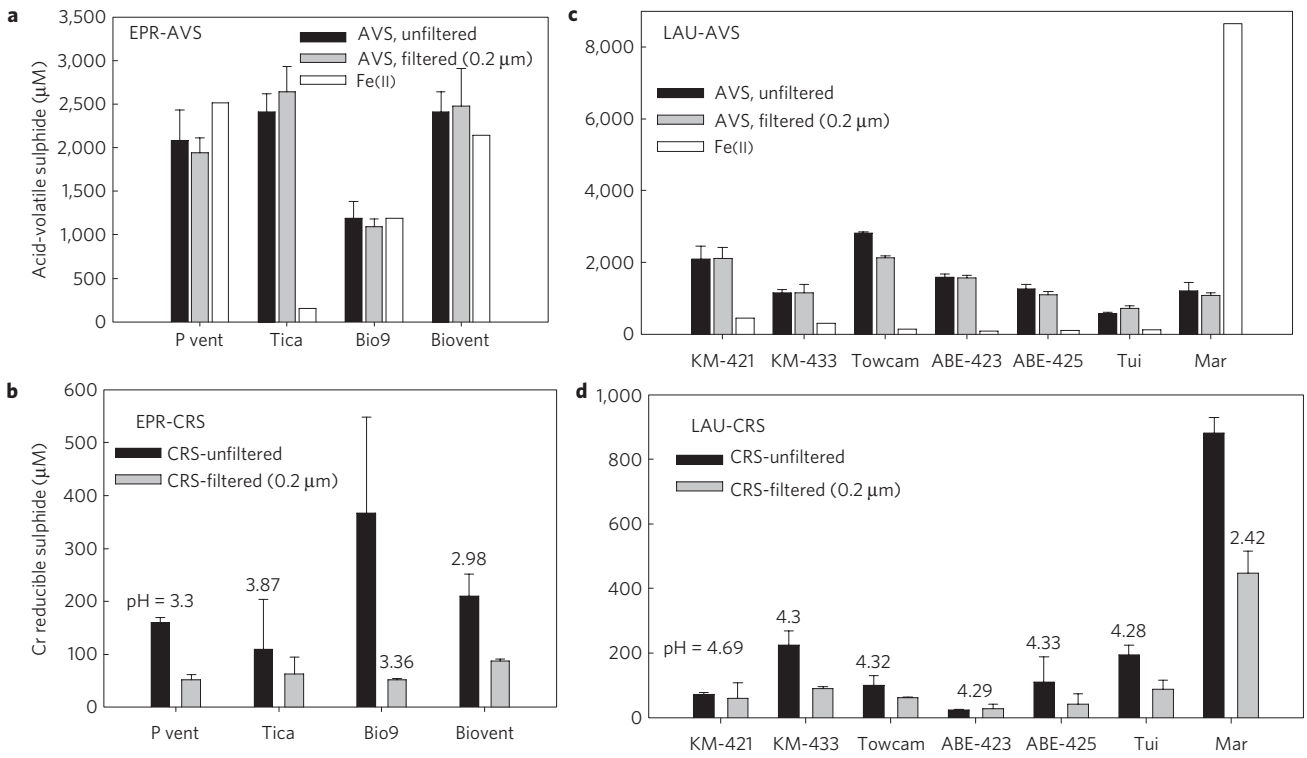

Figure 1 | Sulphide speciation for the vent fluids. Data for EPR, 9° 50′ N (**a** and **b**) and Lau Basin (**c** and **d**) vents. **a** and **c** show acid-volatile sulphide (AVS: $H_2S + FeS$-sulphide) and dissolved Fe and **b** and **d** show chromium-reducible sulphides (CRS—particles containing S_2^{2-}) along with pH values of vent samples. For **c** and **d**, KM: Kilo Moana (421 and 433 indicate samples collected in different dives), Tui: Tui Malila, Mar: Mariner. Measurements were done in triplicate and error bars represent standard deviations from the mean. All concentrations are μM. For dissolved iron (II) measurements, percentage standard deviations remained less than 1%.

Table 1 | Mg concentrations and results of the nitric acid treatment of the vent samples during the Lau 2009 cruise.

Sample ID	Mg	Dissolved Fe, untreated sample	ΔFe-N, unfiltered sample	ΔFe-N, filtered sample	CRS:ΔFe-N, unfiltered sample	CRS:ΔFe-N, filtered sample
Kilo Moana-421	Not measured	464.3	45.4	34.3	1.6	1.8
Kilo Moana-433	4.66	321.4	34.2	27.2	6.6	3.4
Towcam	4.47	152	23.3	18.1	4.4	3.5
ABE-423	3.56	75.8	5.9	4.3	4.3	6.5
ABE-425	3.48	116.2	8.3	6.6	13.3	6.6
Tui Malila	3.25	133.7	7.1	5.6	27.5	16.0
Mariner	8.74	8,648	727.1	221.5	1.2	2.0

ΔFe–N denotes the concentration of Fe measured after nitric acid treatment minus the dissolved iron of the untreated sample. All concentrations are in μM. Of the 21 iron measurements (triplicates for each) shown in this table, the percentage standard deviations of five measurements were between 1% and 0.5% and the rest were less than 0.5%.

known to solubilize pyrite[20]. As shown in Table 1, more iron was measured for all samples using this method, and the difference between untreated and treated samples is shown as ΔFe–N, which gives the concentration of Fe in pyrite nanoparticles. Measured ΔFe–N in filtered samples was 3–12% of the measured iron in untreated samples. This amount is larger than the 4% of the total Fe released from vents that was estimated to be organically complexed as Fe(III) (ref. 3). FeS_2 nanoparticles were highest in the Mariner vent field at 221.5 μM, a concentration higher than the dissolved Fe(II) of many other Lau Basin vents (Table 1). Similar to CRS, more ΔFe–N was found in unfiltered samples. To better constrain the composition of the CRS nanoparticles (that is, to see whether there is a 2:1 sulphur to iron ratio as in FeS_2), the ratio of CRS to ΔFe–N was computed (Table 1). For Kilo Moana and Mariner samples, this ratio is close to or equal to 2, whereas all other samples (<300 °C) had higher CRS:ΔFe–N ratios.

The variability in CRS:ΔFe–N ratios (that is, in the composition of the CRS particles) seems to be correlated with the temperatures of the vents, as shown in Fig. 2. With increasing vent temperature, the CRS:ΔFe–N ratio approaches 2 (in Kilo Moana and Mariner). TEM and SEM-EDX analysis also confirmed the presence of pyrite nanoparticles in the high temperature Kilo Moana vent fluid (see Supplementary Figs S1–S6). Therefore ΔFe–N accounted for CRS in high-temperature vents (>300 °C), whereas the <300 °C vents probably have other chromium-reducible metal sulphides. Metal-sulphide minerals of differing stoichiometries exist, and the S:Fe ratio in these minerals can be as high as 8:1 in fukuchilite

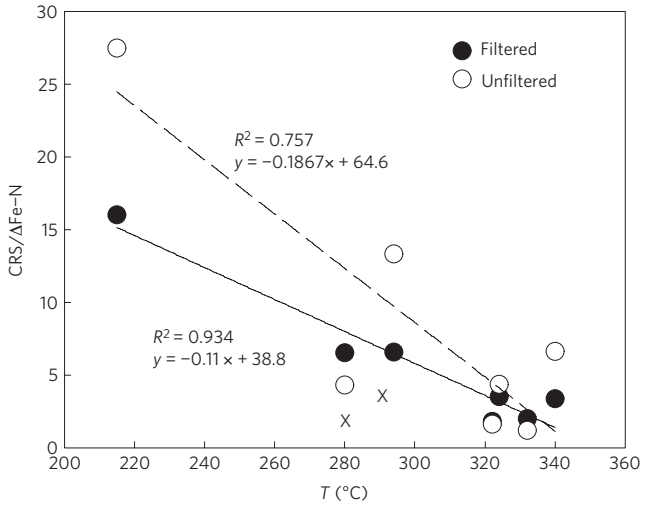

Figure 2 | Temperature of the vent versus the ratio CRS:ΔFe–N. The dashed line is the regression fit for data on unfiltered samples and the solid line is the regression line for the data on filtered samples. The ratio for the filtered samples had a higher correlation of $R^2 = 0.934$. The symbol 'X' is the ratio of CRS to the sum of HNO_3-leachable Fe and Zn for the filtered ABE samples (Zn increased from the HCl to HNO_3 fractions by a factor of two or more in these samples.). Note how the ratio approaches 2 on the consideration of the substitution of Zn for Fe into pyrite nanoparticles.

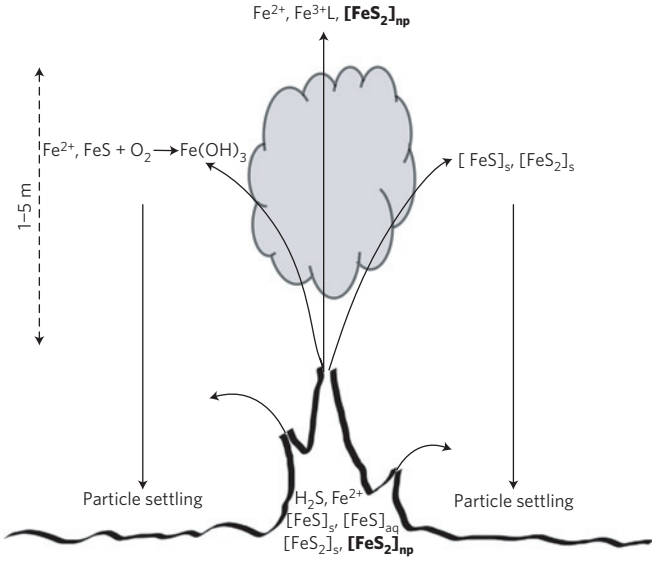

Figure 3 | Pyrite nanoparticles as a previously unrecognized source of iron to the deep ocean. On mixing of the vent fluid with cold, oxic seawater, Fe precipitates primarily as $Fe(OH)_3$ and polymetallic sulphides (the grey cloud represents these precipitates). Pyrite nanoparticles survive the mass precipitation taking place 1–5 m above a chimney and contribute to the iron inventory of the deep ocean. After leaving the discharge zone, the vent-derived iron can exist as Fe(II), organic Fe(III) complexes ('L' stands for organic ligands) and nanoparticle Fe(II) in the form of pyrite nanocrystals, denoted as $[FeS_2]_{np}$.

(Cu_3FeS_8; ref. 21). Copper and zinc have faster water exchange rates than that of Fe, and can also form their own (chromium-reducible) sulphides or coprecipitate with pyrite[15,22]. For instance, our analysis on HNO_3-treated filtered samples of ABE 423 and 425 (temperatures 280 and 294 °C, respectively) revealed the presence of Zn in the HNO_3-leacheable fraction. The concentration of this fraction made the ratio of CRS:(ΔFe–N + ΔZn–N) approach 2 (also shown in Fig. 2), indicating a possible substitution of Zn in pyrite nanoparticles or FeS_2 surrounding ZnS, as found in type III lower temperature chimney deposits[23]. Based on the relation between CRS:ΔFe–N ratio and temperature, the cooling of the hydrothermal fluid in the upflow zone[24] seems to be the primary reason for the difference in formation of pyrite and other chromium-reducible metal sulphide (nano)particles in the vent fluid. In the high-temperature vent fluid, pyrite must be forming through the Berzelius reaction[25,26]:

$$FeS + H_2S \rightarrow FeS_2 + H_2 \quad (1)$$

with the rate law[25]:

$$d[FeS_2]/dt = k[FeS][cH_2S_{(aq)}] \quad (2)$$

The reactant FeS can exist as nanoparticulate FeS or as an ion pair. This reaction could occur in the time between the sampling of the vent fluid and on-board processing (4–24 h). The sample experiences the deep-sea temperature of 2 °C most of this time. Using the actual H_2S and FeS concentrations expected at the pH of the samples, equation (2) and k values in ref. 25, we estimate that the rate of pyrite formation at 2 °C remains less than 1 nM h^{-1}. This indicates that the additional pyrite formed in titanium samplers could range from 0.01–0.3% of the pyrite measured (see Supplementary Fig. S7 and Table 1).

These findings demonstrate that high temperature hydrothermal vents can be significant sources of iron-bearing sulphide (nano)particles to the ocean in addition to Fe(II), which oxidizes to form Fe(III) solids or complexes (Fig. 3). Half-lives for dissolved Fe(II) oxidation at ambient deep-ocean conditions range from minutes (TAG site) to 42 h (Juan de Fuca ridge), whereas at EPR 9° 45′ N, half-lives around 4 h were calculated[13]. The different kinetic results are owing to a combination of differing fluid compositions, deep-water pH and dissolved oxygen content. Kinetic data do not exist for the oxidation of pyrite nanoparticles by O_2 at ambient seawater conditions; however, data exist for the oxidation of other metal sulphide nanoparticles at 25 °C: 30 days for ZnS (ref. 27), 360 days for AgS (ref. 27) and 185 days for CdS (ref. 28; the CdS were also stabilized with organic ligands). Data for micrometre-size pyrite particles were reported in O_2-saturated solutions[29] (pH 7.6–8.6), and <5% of these particles were found to oxidize even after 365 days. Reference 12 also reports the time for complete dissolution of ground and sieved pyrite ranging in particle size from 2 to 100 μm at deep-sea conditions, where 2 μm particles dissolve in 218 days. An extrapolation of the data in ref. 12 gives an estimated minimum 155 days for the complete dissolution of 200 nm size pyrite nanoparticles. Based on these metal sulphide nanoparticle and pyrite microparticle studies, we estimate a half-life range of 1–12 months for pyrite nanoparticles at 25 °C, and 4–48 months at 2 °C, depending on size. These values are much higher than the half-life of dissolved Fe(II) oxidation, indicating that pyrite nanoparticles will survive the oxidation and precipitation that occur when vent fluids meet cold seawater, and thus contribute to the iron inventory in the plumes and away from plumes[10]. As an example, in a non-bouyant plume above the Mid-Atlantic Ridge at 5° S, the concentration of dissolved (<0.4 μm) iron was 20 nM (water depth = 2800 m), whereas the organic ligand concentration was about 4 nM (ref. 3). If we assume that vent fluid containing 50 μM of nanoparticle pyrite-Fe is diluted 10,000 fold[3], it would still have 5 nM of nanoparticulate pyrite-Fe. This amount can account for a substantial fraction of dissolved iron that cannot be explained by organic complexation, as well as much of the Fe anomaly found at the 1–5 km depth range in the South Pacific[10].

Using Stokes' law, we calculated the settling velocity of a spherical pyrite nanoparticle of 200 nm diameter as 4.60×10^{-8} m s^{-1}, or

1.43 m yr^{-1} (see Supplementary Information). For a 2 μm particle, the settling rate becomes 143 m yr^{-1}, and for a 20 μm particle, it is greater than 10 km yr^{-1}, indicating rapid settling for micrometre-size particles, which can be dispersed by plumes up to 2 km away from their source[30]. However, nanoparticles can stay suspended in the deep-sea for years with slower settling rates. They will eventually undergo oxidative dissolution, and then preservation of Fe by organic material[7–9] can further stabilize dissolved Fe.

We conclude that, for $T > 300\,^{\circ}C$ vents, an estimated 10% of dissolved Fe (<200 nm) input from the hydrothermal vents to the deep ocean is in the form of nanoparticulate pyrite. The rates of the formation of pyrite and other metal sulphide nanoparticles in deep-sea hydrothermal vents may be unequalled compared with other natural systems, owing to the high pressure-temperature reaction conditions and the abundance of dissolved sulphide and metals. In this context, the formation and persistence of these metal sulphide nanoparticles in hydrothermal solutions deserve more attention and are of utmost importance if we want to assess the role of vents as natural nanoparticle factories in ocean biogeochemistry.

Methods

The vent fields at the East Pacific Rise (visited in June 2008) were accessed with the human-occupied submersible Alvin and those in Lau Basin (visited in May/June 2009) with the remotely operated vehicle Jason II. The temperature of each vent was measured with a high-temperature probe attached to the submersible. Titanium samplers (also called 'major samplers') were used to sample high-temperature vent fluids[17]. The nozzle of the major sampler was placed 10-15 cm inside the vent orifice to avoid mixing with ambient seawater and ensure the sampling of the actual vent fluid just before it enters the ocean. On retrieval of the sample on board, three replicate subsamples were filtered (200 nm) into 15 ml polypropylene test tubes. Dissolved H_2S in the samples was fixed as follows: 2 ml of both unfiltered and filtered subsamples were added to test tubes containing 2 ml of 0.5 M NaOH. To these, 2 ml of 0.1 M zinc acetate was added. The test tubes were shaken well, with the formation of a white precipitate, and then the fixed sample was frozen immediately at −20 °C. The addition of Zn-acetate causes the precipitation of free sulphide and FeS as ZnS. The amount of Zn added was at least ten times in excess of the expected sulphide concentration of the vent fluid. In our shore-based laboratory, these samples were analysed sequentially for their acid-volatile sulphide (AVS) and chromium-reducible sulphide (CRS) content[18]. Dissolved iron content and pH were measured on board on filtered samples. Ferrozine reagent was used for the colorimetric determination of dissolved iron[19] with a portable spectrophotometer (SP 100V from Analytical Instrument Systems). The filtered sample (50–2,000 μl; volume depends on the concentration of the sample) was added to a test tube containing 7.5 ml deionized H_2O, 0.5 ml concentrated HCl, 1 ml 2.5 M NH_4-acetate and 1 ml 0.01 M ferrozine. Fe(II) stock solution was prepared by dissolving ferrous ammonium sulphate [Mohr's salt— $(NH_4)_2(Fe)(SO_4)_2 6 \cdot H_2O$] in 1% trace metal clean HCl (Optima). Standard solutions for the calibration of the spectrophotometer were prepared in ammonium-acetate buffer as above and calibration was performed daily during the cruise.

During the Lau 2009 cruise, vent fluid samples were also treated with concentrated HNO_3 to solubilize any (nano)particulate pyrite-Fe present in the sample[20]. Five hundred microlitres of concentrated HNO_3 were added to 10 ml of sample. Ten hours after the HNO_3 treatment, samples were analysed for Fe(II) as above. The concentration of Fe always increased after HNO_3 treatment in both unfiltered and filtered samples. The difference between nitric acid-treated and untreated Fe concentrations was denoted as 'ΔFe–N' and gives the concentration of Fe in sulphide particles.

To determine Zn and other metals in the HCl and HNO_3 fractions[20] from 200 nm filtered samples, 40 ml of sample was titrated in a trace metal clean polypropylene Falcon tube with Ar degassed trace metal clean 0.01 M NaOH (ref. 10) to a pH ~8 to promote FeS precipitation and induce other nanoparticulate metal sulphides to co-precipitate with the FeS. The resulting precipitate was separated by centrifugation. Both the filtrate and precipitate were treated with an aliquot of 2 M Optima trace metal grade HCl to obtain a pH 1–2. They were then shaken overnight. For both solution and precipitate in Lau Basin samples, a solid was observed to remain at the bottom of each Falcon tube after reaction with HCl. Immediately before insertion in the ICP-MS, an aliquot of these samples was diluted by a factor up to 20 with a 1% HNO_3/0.5% HCl mix that was prepared from a dilution of trace clean acids with DI water. The solutions were then filtered through a 0.2 μm nuclepore filter into clean tubes, and aliquots were analysed by ICP-MS for total metal in the HCl fraction. This HCl leach is the HCl treated fraction, which is analogous to the AVS sulphide leach.

The Optima HCl treated solution and the remaining precipitates were then treated with Optima HNO_3 and shaken overnight. These solutions were then filtered and aliquots were analysed by ICP-MS, as above, for total metal in the HNO_3 fraction, which is analogous to the CRS sulphide leach.

Received 1 October 2010; accepted 1 April 2011; published online 8 May 2011

References

1. German, C. R. & von Damm, K. L. Hydrothermal processes. *Treatise Geochem.* **6,** 181–222 (2004).
2. Boyle, E. A. *et al.* Iron, manganese, and lead at Hawaii Ocean time-series station ALOHA: Temporal variability and an intermediate water hydrothermal plume. *Geochim. Cosmochim. Acta* **69,** 933–952 (2005).
3. Bennett, S. A. *et al.* The distribution and stabilization of dissolved Fe in deep-sea hydrothermal plumes. *Earth Planet. Sci. Lett.* **270,** 157–167 (2008).
4. Taglibue, A. *et al.* Hydrothermal contribution to the oceanic dissolved iron inventory. *Nature Geosci.* **3,** 252–256 (2010).
5. Boyd, P. W. *et al.* Mesoscale iron enrichment experiments 1993–2005: Synthesis and future directions. *Science* **315,** 612–617 (2007).
6. Mottl, M. J. & McConachy, T. F. Chemical processes in buoyant hydro-thermal plumes on the East Pacific Rise near 21° N. *Geochim. Cosmochim. Acta* **54,** 1911–1927 (1990).
7. Statham, P. J., German, C. R. & Connelly, D. P. Iron(II) distribution and oxidation kinetics in hydrothermal plumes at the Kairei and Edmond vent sites, Indian Ocean. *Earth Planet. Sci. Lett.* **236,** 588–596 (2005).
8. Schmidt, K., Koschinsky, A., Garbe-Schonberg, D., de Carvalho, L. M. & Seifert, R. Geochemistry of hydrothermal fluids from the ultramafic-hosted Logatchev hydrothermal field, 15° N on the Mid-Atlantic Ridge: Temporal and spatial investigation. *Chem. Geol.* **242,** 1–21 (2007).
9. Toner, B. M. *et al.* Preservation of iron (II) by carbon-rich matrices in a hydrothermal plume. *Nature Geosci.* **2,** 197–201 (2009).
10. Wu, J., Wells, M. L. & Remember, R. Dissolved iron anomaly in the deep tropical–subtropical Pacific: Evidence for long-range transport of hydrothermal iron. *Geochim. Cosmochim. Acta* **75,** 460–468 (2011).
11. Elderfield, H. & Schultz, A. Mid-ocean ridge hydrothermal fluxes and the chemical composition of the ocean. *Annu. Rev. Earth Planet. Sci.* **24,** 191–224 (1996).
12. Feely, R. A. *et al.* Composition and dissolution of black smoker particulates from active vents on the Juan de Fuca Ridge. *J. Geophys. Res.* **92,** 11347–11363 (1987).
13. Field, M. P. & Sherrell, R. M. Dissolved and particulate Fe in a hydrothermal plume at 9° 45′ N, East Pacific Rise: Slow Fe(II) oxidation kinetics in Pacific plumes. *Geochim. Cosmochim. Acta* **64,** 619–628 (2000).
14. Luther, G. W. *et al.* Chemical speciation drives hydrothermal vent ecology. *Nature* **410,** 813–816 (2001).
15. Hsu-Kim, H., Mullaugh, K. M., Tsang, J. J., Yucel, M. & Luther, G. W. Formation of Zn- and Fe-sulphides near hydrothermal vents at the Eastern Lau Spreading Center: Implications for sulphide bioavailability to chemoautotrophs. *Geochem. Trans.*, **9,** 6 (2008).
16. Von Damm, K. L. in *AGU Geophysical Monograph 144. The Subsurface Biosphere at Mid-Ocean Ridges* (eds Wilcock, W. S. D., DeLong, E. F., Kelley, D. S., Baross, J. A. & Cary, S. C.) 245–268 (American Geophysical Union, 2004).
17. Von Damm, K. L. *et al.* Chemistry of submarine hydrothermal solutions at 21° N, East Pacific Rise. *Geochim. Cosmochim. Acta* **49,** 2197–2220 (1985).
18. Fossing, H. & Jørgensen, B. B. Measurement of bacterial sulphate reduction in sediments: Evaluation of a single step chromium reduction method. *Biogeochemistry* **8,** 205–222 (1989).
19. Stookey, L. L. Ferrozine—a new spectrophotometric reagent for iron. *Anal. Chem.* **42,** 779–781 (1970).
20. Huerta-Diaz, M. A. & Morse, J. W. Pyritization of trace metals in anoxic marine sediments. *Geochim. Cosmochim. Acta* **56,** 2681–2702 (1992).
21. Vaughan, D. J. & Craig, J. R. *Mineral Chemistry of Metal Sulphides* (Cambridge Univ. Press, 1978).
22. Morse, J. W. & Luther, G. W. Chemical influences on trace metal-sulphide interactions in anoxic sediments. *Geochim. Cosmochim. Acta* **63,** 3373–3378 (1999).
23. Koski, R. A., Jonasson, R. I., Kadko, D., Smith, V. K. & Wong, F. L. Compositions, growth mechanisms, and temporal relations of hydrothermal sulphide–sulphate–silica chimneys at the northern Cleft segment, Juan de Fuca Ridge. *J. Geophys. Res* **99,** 4813–4832 (1994).
24. Tivey, M. K. The influence of hydrothermal fluid composition and advection rates on black smoker chimney mineralogy: Insights from modeling transport and reaction. *Geochim. Cosmochim. Acta* **59,** 1933–1949 (1995).
25. Rickard, D. T. Kinetics of pyrite formation by the H_2S oxidation of iron (II) monosulphide in aqueous solutions between 25 and 125 °C: The rate equation. *Geochim. Cosmochim. Acta* **61,** 115–134 (1997).
26. Rickard, D. T. & Luther, G. W. Kinetics of pyrite formation by the H_2S oxidation of iron (II) monosulphide in aqueous solutions between 25 and 125 °C: The mechanism. *Geochim. Cosmochim. Acta* **61,** 135–147 (1997).

27. Luther, G. W. & Rickard, D. T. Metal sulphide cluster complexes and their biogeochemical importance in the environment. *J. Nanopart. Res.* **7,** 389–407 (2005).
28. Mullaugh, K. M. & Luther, G. W. Growth kinetics and long-term stability of CdS nanoparticles in aqueous solution under ambient conditions. *J. Nanopart. Res.* **13,** 393–404 (2011).
29. Nicholson, R. V., Gillham, R. W. & Reardon, E. J. Pyrite oxidation in carbonate-buffered solution 2. Rate control by oxide coatings. *Geochim. Cosmochim. Acta* **54,** 395–402 (1990).
30. Feely, R. *et al.* Composition and sedimentation of hydrothermal plume particles from North Cleft segment, Juan de Fuca Ridge. *J. Geophys. Res.* **99,** 4985–5006 (1994).

Acknowledgements

This work was supported by grants to G.W.L. III from the National Science Foundation RIDGE program and the University of Delaware's NSF EPSCoR program. A.G. acknowledges support from the Critical Zone research program funded by the University of Delaware. We thank E. Croker for assistance with SEM imaging, S. Modla for assistance with TEM imaging and C. Golt for assistance in ICP analyses.

Author contributions

M.Y. and G.W.L. III designed the study. M.Y., A.G. and G.W.L. III performed sample collection and on-board processing. M.Y. performed sulphide and iron speciation analyses. A.G. performed other metal analyses and reaction kinetics calculations. C.S.C. performed TEM analysis of pyrite nanoparticles and contributed to data analysis. M.Y. and G.W.L. III drafted the manuscript. All authors contributed to interpretation of the results and editing of the manuscript.

Additional information

The authors declare no competing financial interests. Supplementary information accompanies this paper on www.nature.com/naturegeoscience. Reprints and permissions information is available online at http://www.nature.com/reprints. Correspondence and requests for materials should be addressed to M.Y. or G.W.L. III.